Supplemental Document

Snapshot hyperspectral light field tomography: supplement

QI CUI, JONGCHAN PARK, YAYAO MA, AND LIANG GAO*

Department of Bioengineering, University of California Los Angeles, Los Angeles, California 90095, USA
**Corresponding author:* *gaol@ucla.edu*

Supplement DOI: https://doi.org/10.6084/m9.figshare.16918231

Parent Article DOI: https://doi.org/10.1364/OPTICA.440074

Snapshot Hyperspectral Light Field Tomography: supplemental document

1. Dove prism and cylindrical lens array design

The pictures of the mounts that hold the dove prisms and cylindrical lenses are shown in Fig. S1, where the numbers indicate the rotation angles in degrees of dove prisms. Instead of arranging the dove prisms in a rectangular array, we chose a near circular pattern to fulfill the aperture of the main lens. Each dove prism rotates the perspective image at the corresponding pupil location, which is further imaged by a cylindrical lens.

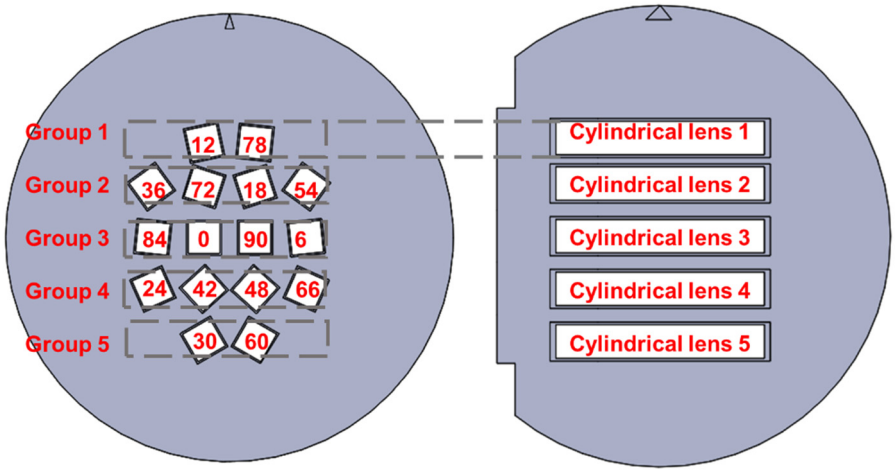

Fig. S1. Mounting plates that hold the dove prisms and cylindrical lenses. The numbers in the left panel indicate the rotation angles of dove prims in degrees. The dove prisms are divided into five group, each passing the light to the same cylindrical lens.

2. Spectral and depth calibration

To calibrate the spectral response, we placed a pinhole (Thorlabs, P50D) at the nominal object plane and illuminated it with monochromatic light of different wavelengths. The corresponding pixel locations of the projections were recorded. Because the dispersion curve of a diffraction grating is linear, five wavelengths provide a fitting with negligible localization errors (Fig. S2(b), top). Because 1 nm bandwidth in wavelength occupied four pixels on the camera, the system provides a spectral resolution of 0.25 nm.

To calibrate the depth, we put a pinhole (Thorlabs, P50D) at the front focal plane of the objective lens, scanned the pinhole from -3.75 mm to 3.75 mm along the depth axis with a 0.625 mm step, and captured an image at each depth. Next, we digitally refocused each pinhole image by tuning the shearing parameter, which is defined in Section 2.C. For each pinhole image, we identified the shearing parameter that best brings the image back in focus and recorded corresponding physical depth. The best focus image can be found by maximizing a focus measure (e.g., sum of modified Laplacian) for each pixel of the image [1]. We fitted the curve with a linear model. The resultant shearing to depth curve is shown in the bottom figure in Fig. S2(b). Using this curve, we can digitally refocus a 3D objective, and the corresponding depth can be deduced based on the shearing parameter.

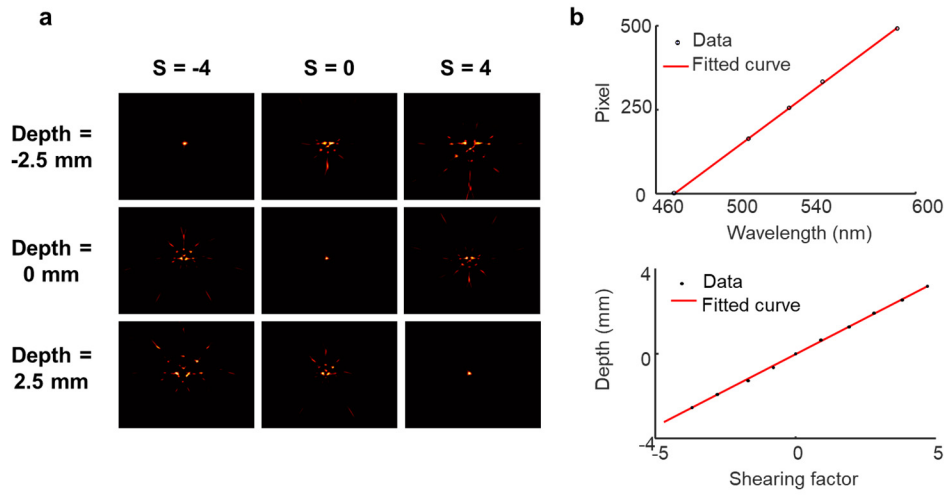

Fig. S2. Spectral and depth calibration. (a) Three example pinhole images refocused with different shearing factors. The pinhole images were captured at different depths. (b) Measured chromatic dispersion curve and shearing to depth relation.

3. Lateral and axial resolution

We quantified the resolution under the sparse condition by imaging a point object (a 10 μm pinhole). The lateral and axial resolution resolutions are measured as the full width half maximum (FWHM) of the impulse response along the lateral and axial direction, respectively (Fig. S3). The measured lateral and axial resolutions are 22 μm and 1 mm, respectively.

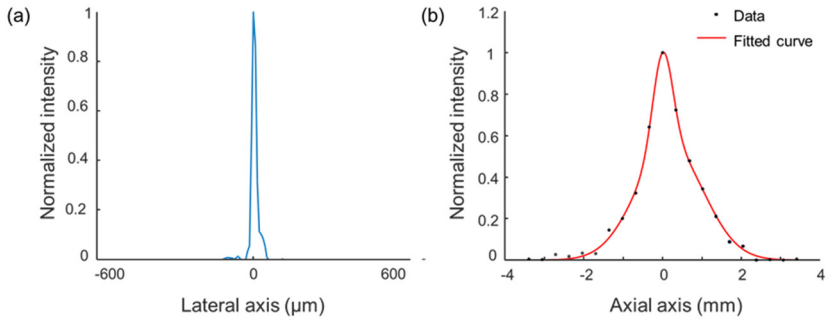

Fig. S3. Characterization of spatial and axial resolutions. (a) Lateral intensity distribution of a reconstructed 10 μm pinhole. (b) Axial intensity distribution of a reconstructed 10 μm pinhole, fitted with a Gaussian model.

4. Numerical refocusing of an object at different depths

We placed an object at depth = -3.75 mm, 0 mm, 3.75 mm with respect to the nominal focal plane of the Hyper-LIFT camera. At each object position, we captured a snapshot and generated the focal stack images. Fig. S4 (a), (b) and (c) show the sweeping of the focal plane images at the corresponding object setting. As expected, the object appears in focus only at its designated location. Noteworthily, the out-of-focus image in LIFT cameras appear as ghost images rather than uniformly radial blur as in conventional widefield imaging. This effect has been discussed in our previous publication [1].

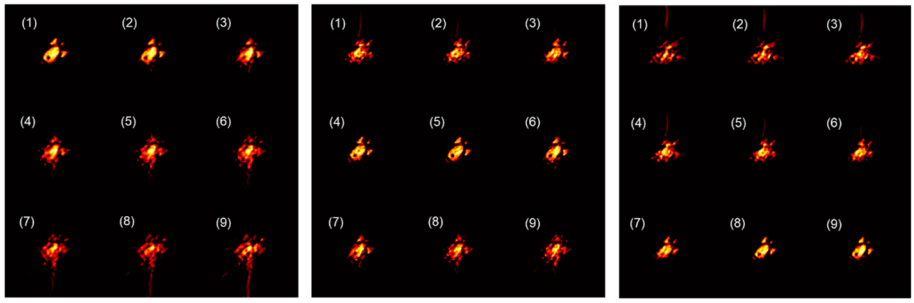

(a) Object positioned at depth = -3.75 mm

(b) Object positioned at depth = 0 mm

(c) Object positioned at depth = 3.75 mm

Fig. S4. Sweeping of focal stack images for an object positioned at three depths. The numbers in the subpanels denote the indices of the shearing parameter. From (1) to (9), refocusing depth is from – 4 mm to 4 mm, with step size = 1 mm.

References

1. X. Feng, L. Gao. "Ultrafast light field tomography for snapshot transient and non-line-of-sight imaging," Nat. Commun 12, 2179 (2021).